International Communications in Heat and Mass Transfer 127 (2021) 105502

Contents lists available at ScienceDirect

International Communications in Heat and Mass Transfer

journal homepage: www.elsevier.com/locate/ichmt

Heat and mass transfer of evaporative cooler with elliptic tube heat exchangers- an experimental study

Liang-Han Chien [a,b], De-Cian Chen [a,b], Yu-Jie Liu [a,b], Wei-Mon Yan [a,b,*], Mohammad Ghalambaz [c,d,**]

[a] Department of Energy and Refrigerating Air-Conditioning Engineering, National Taipei University of Technology, Taipei 10608, Taiwan
[b] Research Center of Energy Conservation for New Generation of Residential, Commercial, and Industrial Sectors, National Taipei University of Technology, Taipei 10608, Taiwan
[c] Metamaterials for Mechanical, Biomechanical and Multiphysical Applications Research Group, Ton Duc Thang University, Ho Chi Minh City, Viet Nam
[d] Faculty of Applied Sciences, Ton Duc Thang University, Ho Chi Minh City, Viet Nam

ARTICLE INFO

Keywords:
Heat and mass transfer
Closed-loop cooling system
Elliptic tube heat exchanger
Water sprinkler

ABSTRACT

In the present study, an evaporative cooling test system consisting of an elliptical-heat exchanger was examined. Tests were conducted for various airflow rates of 52, 68, 81, 96 Cubic Meter per Minute (CMM), sprinkler water flow rates of 30, 40, 50 Liter per Minute (LPM), and hot water flow rates of 18, 22, 28 LPM. The sprinkle nozzle types and outside wet-bulb temperatures were also investigated. The convective heat transfer of the sprinkle water film outside the tubes and the mass transfer between air and water film on tube bundles were probed. The film thickness and sprinkle water picture were studied using high-speed cameras and image processing techniques. The results show that the mass transfer performance of the evaporative cooler was enhanced with the growth of the airflow rate. When the sprinkler water flow rate rose to 50 LPM, the heat-mass transfer coefficient of the evaporative cooler decreased since the water film on the tube was thickened. The low hot water flow rate at the tube side (18 LPM) resulted in a superior performance due to a high local temperature and improved local mass transfer. The experimental data were used to obtain empirical correlations for the heat coefficient of the liquid film and mass transfer.

1. Introduction

The cooling systems are an essential part of many industrial plants [1], power systems [2], and water distillation systems [3]. The heat dissipation mechanism of evaporative cooling technology can be divided into three parts of the heat and mass transfer characteristics (mass transfer coefficient) of the liquid-air interface, the heat transfer characteristics of the sprinkle water film outside the pipe (heat transfer coefficient of the liquid film), and the heat transfer characteristics of the internal fluid (convection heat transfer coefficient in the tube). The evaporative cooling in the present study is a close loop cooling system, in which the hot water flows inside tubes while the cold water and airflow pass outside of the tubes.

When air passes through a wet surface and evaporation occurs, two mechanisms of sensible heat exchange and latent heat exchange occur. Sensible heat exchange is the result of the temperature difference between air and water, and the latent heat exchange (mass transfer phenomenon) is due to the concentration difference. The heat transfer rate is the sum of the sensible heat exchange capacity and the latent heat exchange capacity. There are also recent patents on evaporative cooling systems. For instance, Moses [4] proposed a capable indirect cooling system for buildings that could link outdoor and indoor intermediate fluid systems when circumstances allow. Bourgeois [5] invented an evaporative system that could quickly cool a pot or boiler. Many scientific aspects of evaporative cooling systems, such as the paving materials [6,7], sub-wet bulb temperature cooling [8], and hybrid evaporative systems for reduction of water consumption [9], have been addressed recently. Moreover, various new applications for evaporative cooling systems have been established recently. The evaporative cooling

* Correspondence to: Wei-Mon Yan, Department of Energy and Refrigerating Air-Conditioning Engineering, National Taipei University of Technology, Taipei 10608, Taiwan.
** Correspondence to: Mohammad Ghalambaz, Metamaterials for Mechanical, Biomechanical and Multiphysical Applications Research Group, Ton Duc Thang University, Ho Chi Minh City, Viet Nam.
E-mail addresses: wmyan@ntut.edu.tw (W.-M. Yan), mohammad.ghalambaz@tdtu.edu.vn (M. Ghalambaz).

https://doi.org/10.1016/j.icheatmasstransfer.2021.105502

Available online 12 August 2021

Nomenclature

Latin symbols

A_o	overall area of the tubes array
c_p	specific heat
d	diameter of the tube, differential operator
D	the hydraulic diameter of the elliptical tube
f	dummy variable
h	convective heat transfer coefficient
h_{sen}	sensible convective heat transfer coefficient
i	enthalpy
i_a'	saturated air enthalpy
k	thermal conductivity
K_m	mass transfer coefficient
Le_f	Lewis number
$\dot{m}$	mass flow rate
n_r	number of tubes in each row of the array
Nu	Nusselt number
Pr	Prandtl number
q	heat transfer rate
Q_a	total absorbed heat by the airflow
Q_c	cooling capacity
R	strain number
Re	Reynolds number
T	temperature
$\overline{T}$	average temperature
u	velocity
U_{film}	heat transfer coefficient
w	humidity
x	independent variables

Greek symbols

α	thermal diffusivity
Γ	parameter defined by $\frac{\dot{m}_w}{2n_r \cdot 2L_t}$
θ	the performance index
μ	dynamic viscosity
ρ	density
ω	error estimation

Subscripts

f	liquid
g	vapor
int	liquid-gas interface
lat	latent heat
m	average, mass transfer
o	outside, exit
s	sprinkle
sen	sensible heat
i	inside, entrance
h	hot water
WB	wet-bulb
t	tube
w	water
max	maximum

Table 1
Specifications of evaporative coolers in the present study and the literature works.

Specifications	Present study	Fang [36]	Zheng et al. [27]	Niitsu et al. [34]	Mizushima et al. [35]	Hasan and Sirén [23]	Hasan and Sirén [37]
Tube type	Elliptical	Elliptical	Elliptical	Circular	Circular	Circular	Circular
Long axis (mm)	20.65	20.65	31.8	16	12.7/19.05/40	10	10
Short axis (mm)	10.2	10.2	21.6	16	12.7/19.05/40	10	10
Length (m)	0.6	0.6	1.2	0.4	0.5	1.2	0.88
Number of columns	12	8	8	8	8	19	
Number of tubes in row	12	8	37	20	6	12	
Horizontal spacing (mm)	31.2	31.2	44	38.1	25.4/38.1/80	20	28
Vertical spacing (mm)	34.8	34.8	64	37.5	–	60	

with forced circulation of coolant for electronic components [8], cooling tower in underground engineering [10], solar-powered evaporative cooling storage system for tropical fruits and vegetables [11], and evaporative cooling of data centers [12] are just a few examples.

Cuce and Riffat [13] performed a comprehensive review of the evaporative cooling systems for building applications and reported a large potential to save energy in hot and arid climatic zones by utilizing evaporative cooling systems. Kojok et al. [14] performed a comprehensive review of the hybrid cooling systems. The authors found that hybrid cooling systems could provide multi advantages, but they should match the conditions of a climate zone. Sharma and Sharma [15] explored the literature studies concerning the evaporative condensers for improving the heat transfer efficacy of domestic air conditioners. They found that the evaporative systems could improve the COP of air conditioners. Very recently, Yang et al. [16] reviewed the recent developments in evaporative cooling systems and enhancement methods. They reported that employing membranes, desiccants, and the combination of membranes and desiccants could enhance the evaporative cooling systems. The novel mechanisms for the improvement of evaporative cooling systems could be classified into direct vs. indirect evaporative cooling [17] and desiccants evaporative cooling [18]. The energy-water-environment and reduction of water energy consumption in cooling systems is another important aspect of cooling systems, which should be taken into account [19–21]. Currently, 15% of global fresh water was consumed for power generation the water destilation [22].

Considering the evaporative cooling systems, Hasan and Sirén [23] utilized a closed cooling water tower prototype for cooling an office building. They installed the cooling unit on the ceiling of the building to reduce the indoor heat load. The specifications of the prototypes are summarized in Table 1. The outer diameter of the tubes was 10 mm, and the length of the tubes was 1.2 m. The cooling system was a 10 kW nominal power, and the impact of airflow rate and the number of tubes on the heat transfer and coefficient of performance (COP) was studded. The results show that the increase of the airflow rate or the number of tubes increases the heat removal and decreases the COP.

In the closed wet cooling tower systems, the hot working fluid is not in direct contact with the cooling water and ambient air. Hasan and Sirén [23] established an experimental test system consisting of three cycles of air-side circulation, hot water circulation inside the tubes, and water sprinkle circulation outside the tubes. The cooling water system sprinkles water on the surface of the heat exchanger tubes through a nozzle. A fan passes the air over the heat exchanger tubes while the tubes were supported with 12 fins. The fin thickness and pitch were 0.5 mm and 12 mm, respectively. In their experiment, the air mass rates were

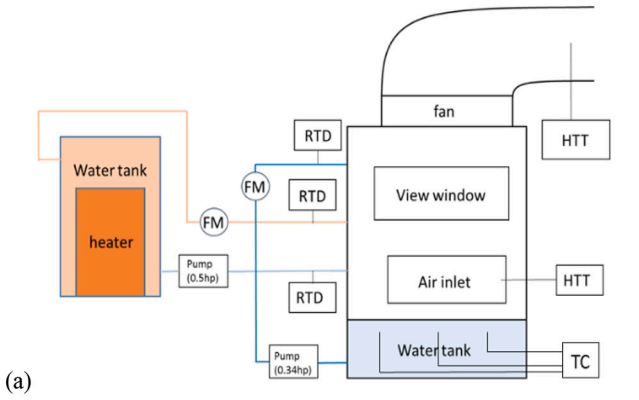

(a)

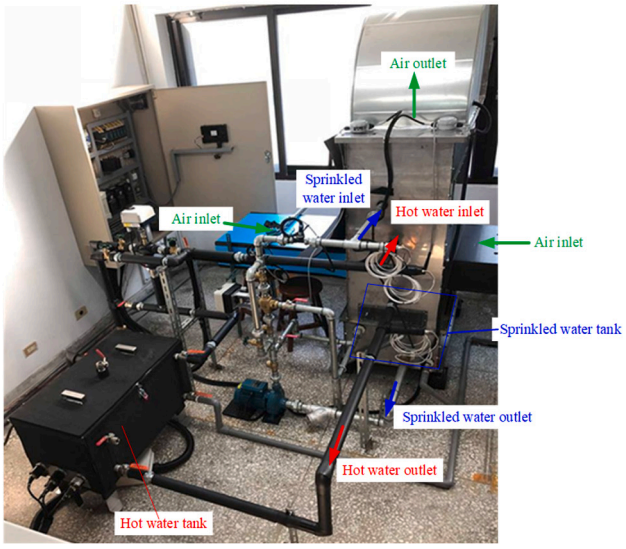

(b)

Fig. 1. (a) Schematic diagram of the experimental setup and measurement locations, (b) photo of the experimental setup.

0.0151, 0.0235, and 0.0323 kg/s. Hot water flow in the tube was 0.114 kg/s, and the hot water temperature in the tube was tested at 30, 32, and 34 °C. The results showed a notable improvement in the heat transfer rate by using the plate-finned tubes. The outcome demonstrated that sprinkling water over the tubes reduces the fin efficiency compared to a dry air blow. The authors also found that although fins could improve the heat transfer rate, they can boost the pressure drop. Hence, the energy index (the ratio of volumetric thermal conductance to air pressure-drop per unit length) remained the same for two cases of a finned heat exchanger and a simple heat exchanger.

Facao and Oliveira [24] proposed a closed wet cooling tower for chilled ceilings in buildings. They investigated the effect water-sprinkle flow-rate of the closed-loop evaporative cooling system on the system's thermal performance. The results show that the sprinkle flow rate has minimal influence on tower efficiency. The growth of the sprinkle flow rate enhances the efficiency up to a certain level, and further raising the flow rate only slightly contributes to efficiency improvement. Hence, they concluded that there is an optimum sprinkle flow rate for the best efficiency. Heyns and Kröger [25] investigated the evaporative cooling of a closed-loop system consisting of 15 tube rows with eight tubes as each row. The length of the tubes was 0.65 m, and they were placed in a triangle arrangement. They measured the water temperatures of the hot inlet and outlet, the sprinkler, the sprinkler between each array. They found that a sprinkler flow of 1.7 kg/m^{2}s was required to keep all pipes uniformly wet. The difference between the sprinkler temperature and the average sprinkler temperature in all experimental results was less than 3 °C. Both the liquid film heat transfer coefficient and the mass transfer coefficient were increased by increasing air and sprinkler flow rates. In another study, Hasan and Siren [26] tested circular and elliptical tube arrays under the same experimental conditions, and they investigated the thermal performance of the circular and elliptical tubes. The average thermal performance for the elliptical tube was 79% of that for the circular tube. However, the elliptical tubes induce a lower pressure drop and frictional factor. The overall performance of the elliptical tubes was 1.93–1.96 times that for the circular tube. Hence, the elliptical tubes could of practical interest in wet closed-loop cooling systems. Zheng et al. [27] established an innovative elliptical tube closed-loop cooling water tower. The temperature of the hot water pipeline at the entrance of the cooling tower was measured with PT100 sensors, and the flow of hot water and sprinkler water was measured with an electromagnetic flow meter. The liquid film heat transfer and mass transfer coefficient of water on the sprinkle side was studied. The experimental results show that the heat transfer coefficient of the water-film is a function of the water and air mass flow rates. Here, as a brief summary of the literature works, the specifications of the previous studies are summarized in Table 1.

The closed wet cooling tower systems may not be advantageous for energy saving compared to an open system such as a swamped cooler. Direct contact between the hot water and the ambient air in an open-loop cooling water system such as a swamp cooling system could be much more energy-efficient than a closed wet cooling system. However, in the current system, the hot liquid is not in direct contact with the cooling water, and hence, the hot water loop remains clean and closed. Thus, the closed wet cooling tower systems are of technological interest where the hot liquid should not be in direct contact with the ambient air. Therefore, any heat transfer improvement in a closed wet cooling tower could be of great interest since it can lead to significant water and energy saving.

Sarker et al. [28] explored the thermal behavior of a closed wet cooling tower where the cooling tower was made of a copper coil (outer diameter of 15.88 mm). The coil's tubes were circular with no fins. The closed wet cooling towers with circular tubes were also investigated by Niu et al. [29], Zhu et al. [30], Nugraha [31], and Rashidinejad et al. [32].

As seen, few studies investigated the thermal behavior of closed-loop wet cooling systems by using elliptical tubes. The present experiment aims to address the impact of water sprinkling flow rates, nozzle types, the hot water flow rate, and outside wet-bulb temperature on the thermal behavior and performance index of a new prototype closed-loop cooling system made of elliptical tubes.

2. Experimental setup and methods

In a closed system, the hot water circulates inside the elliptical tubes of the heat exchanger and loses its heat to a spray of cooling water and airflow, which cools down the external surface of the elliptical tubes. The details of the experimental setup and methods will be discussed here.

2.1. Experimental setup

The present experimental setup could be divided into three major loops of hot water circulation, spray water circulation, and air circulation. The schematic view of the experimental setup is plotted in Fig. 1(a), while an actual image of the setup is depicted in Fig. 1(b). As seen in Fig. 1(a), the water was heated in a water tank using a heater, and a pump circulates the water inside an elliptical-tube heat exchanger to be cooled down. A sprinkler of cold water drops over the external surface of the tubes and cools the external surface of the elliptical-tube heat exchanger. The sprinkled-water then drops to the bottom to be collected in a water tank.

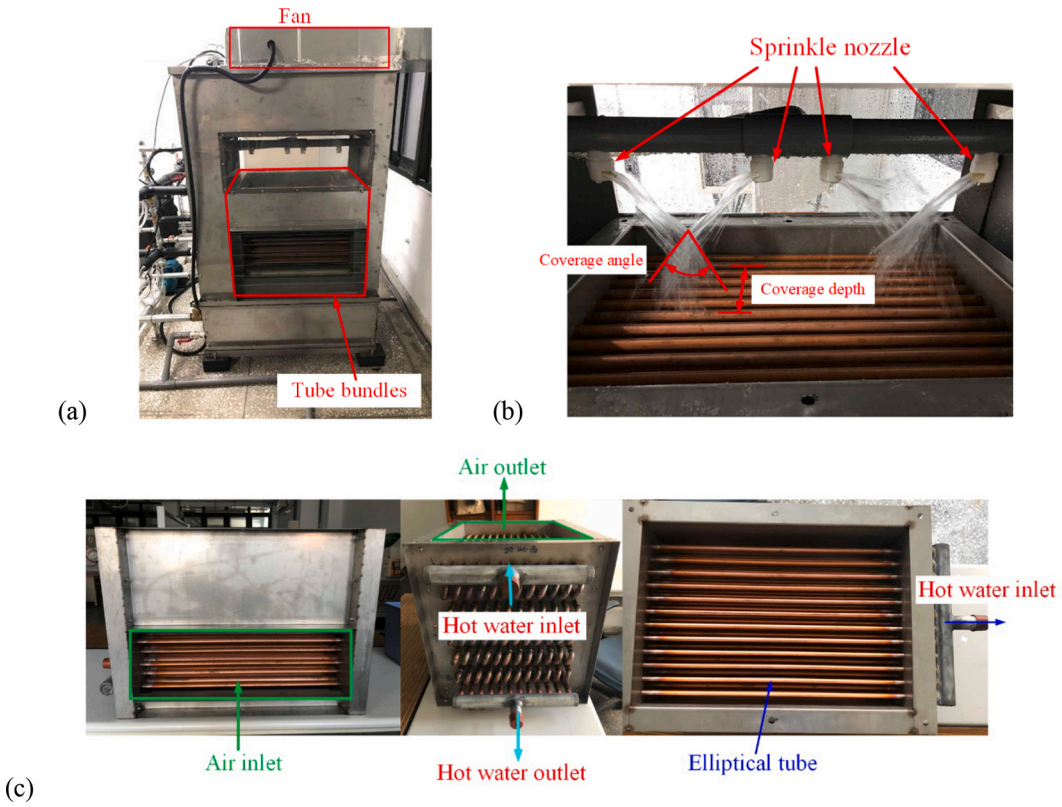

Fig. 2. The prototype and its components, (a): a photo of the prototype, (b): interaction between the spraying water and heat exchanger, (c): an array of elliptical tubes.

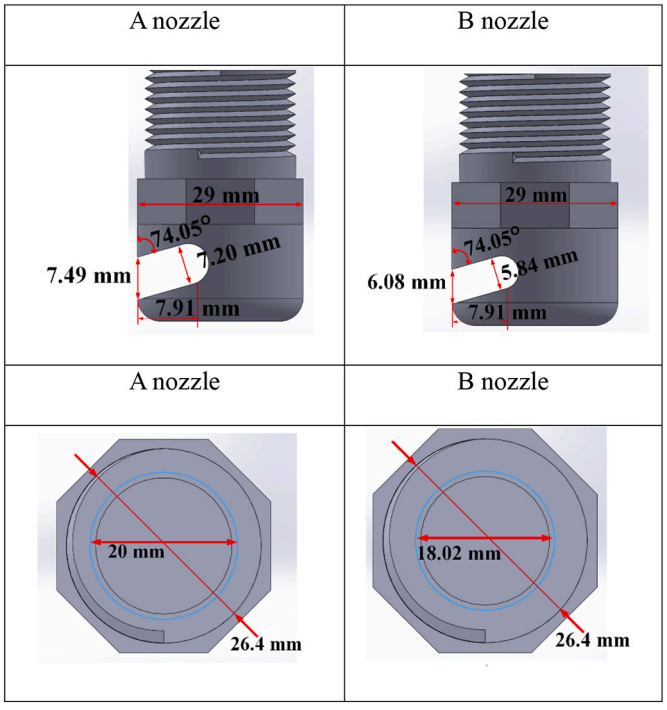

Fig. 3. The geometrical specifications of the adopted nozzles.

A pump sinks the water from the collection tanks and sends it to the top to be sprinkled again. An axial fan was mounted at the top of the experimental setup, which provides fresh airflow for cooling the sprinkling water. This way, the cooling system, which consists of the air cooling and the sprinkler, was separated from the hot water system. The water sprinkle, air cooling flow, and hot water tubes were placed inside a shell, referred to as a prototype. A close view of the prototype is illustrated in Fig. 2(a). The interaction between the cooling system and hot water system takes place at an elliptical tube heat-exchanger, as shown in Fig. 2 (b).

The main components of the prototype are an array of elliptical tubes, a stainless steel shell, a water sprinkler loop, nozzles, and an axial flow fan. A photo of the array of elliptical tubes is exhibited in Fig. 2 (c). As seen, the tubes were connected by using U-shaped elbows and fixed in their places by stainless steel plates. The details of the tubes and their arrangements are presented in Table 1. The shell of the prototype was assembled by using laser-cut stainless steel plates. The plates were made of #304 stainless steel with a thickness of 1.5 mm. The arrays of tubes, nozzles, and measurement instruments were placed in the shell. Several windows were embedded at the sidewalls of the shell. The windows are covered with transparent acrylic and used for observation purposes. At the bottom of the prototype, the water tank was equipped with a floating ball automatic water replenishment device. There were side maintenance hatches, which provide access into the shell for cleaning purposes. The fan was installed at the top of the prototype for air circulation purposes.

The water sprinkler system is composed of a pump, pipelines, a frequency converter, and a proportional three-way valve. The frequency converter and the proportional valve control the flow rate of water in the sprinkler system. The pump (model: NM4 25 made by CALPEDA) is a 3 phase 220 V/0.34HP, with a maximum flow rate of 100 LPM and a minimum head of 3.6 m. A Y-type filter was installed in front of the suction side to filter impurities in the water and avoid damaging the pump. For flow control purposes, a proportional three-way valve was placed at the exit end of the pump. The air-side circulation is composed of a fan, a prototype, and an air duct. The fan draws waste heat out of the prototype in the exhaust air and guides it to the outside through the air

Table 2
Specifications of measuring instruments.

Measuring instrument	Quantity	Model	Specification
Resistance thermometer	3	Four-wire PT100	Measurement range: −200 °C ~ 200 °C temperature correction range: 20 °C ~ 50 °C accuracy: ± 0.046 °C
Thermocouple	3	T-type	temperature correction range: 20 °C ~ 35 °C
Temperature and humidity transmitter	1	Dwyer Model 657–1	Temperature measurement range: 0– 100 °C accuracy: ±0.5 °C Relative humidity measurement range: 0– 100% accuracy: ±3%(0–10%, 90–100% RH)
Temperature and humidity transmitter	1	TRH300	Temperature measurement range: 0– 100 °C accuracy:±0.3 °C Relative humidity measurement range: 0– 100% accuracy: ±2%
Turbine flowmeter	2	Hubatype210	Measurement range: 3– 150 LPM accuracy: 1%(full scale)
Pitot tube	10	Dwyer Model 607–01	Diameter 5/16″, length 8”
Differential pressure gauge	10	Cole-Parmer 68,333–24	Measurement range: 0– 1”WC, Error 0.4%
Power Analyzer	1	HIOKI/3169–20	measurement range:150– 600 V , 0. 5– 500 A 0.075– 900 kW Accuracy: effective power ± 0.2%
Speed Camera	1	MEMRECAM HX-7 s	2560 × 1920 pixel @850 fps 1920 × 1080 pixel @2000 fps Maximum 200,000 fps Sensitivity ISO 80000 (Mono)

Table 3
Test conditions and corresponding Re_a, Re_w, Re_h for the study of the A when the sprinkle flow rate of 40 LPM (50 Hz).

Experiment frequency (Hz)	30	40	50	60
Air volume (CMM)	52.74	68.23	81.52	96.20
Re_a	5240.05	6788.04	8109.93	9564.76
Sprinkle flow rate (LPM)	40.92	40.80	40.71	40.53
Re_w	119.59	115.64	111.74	109.39
Hot water flow rate (LPM)	27.81	27.90	27.96	27.95
Re_h	5167.08	5034.95	4903.21	4826.07
Outside air wet bulb temperature (°C)	23.52	23.38	23.12	23.09

duct to avoid short-term circulation caused by air remaining inside the heat exchanger. An inverter was used to control the fan speed and the airflow rate in the prototype. The blower (manufactured by ZIEHL-ABEGG) is a 3-phase 220 V/1 hp. with an airflow rate of 4100 CMH/ static pressure170 Pa.

The adopted nozzles in the sprinkler system are two types: A nozzle and B nozzle, which their geometrical specifications are summarized in Fig. 3. The coverage angle and coverage depth are 36.22–112.74° and 40.99–84.53 mm, respectively, for A nozzle. While for B nozzle, the coverage angle and coverage depth are 65.17–113.79° and 71.84–85.75 mm, respectively. The operating pressure ranges from 153.7 to 157.6 kPa。.

As seen, the nozzles are flat with large diameters, which could resist impurities and clogging issues. In the present experiment, a total of four nozzles with a distance of 20 mm were employed. An image of the sprinkling behavior of nozzles is depicted in Fig. 2(b). The heating water tank was applied as a simulated load during the experiment. Five electric heating tubes were placed inside the water tank. Each element provides a heating power of 2.6 kW, and hence, the total heating power was 13 kW. The water tank holds a total volume of 96 L of water while and an automatic float water refilling device.

2.2. Measurements

The measurements include monitoring temperatures at the inlet and outlet of the hot water loop, air inlet and outlet temperatures and relative humidity, hot water and sprinkle water flow rates, and power consumption. A data logger was employed to read and record the measurements. The hot water inlet and outlet of the prototype were measured using resistance thermometers (RTD), which were placed at the inlet and outlet of the hot water pipes. The temperature of the sprinkler outlet and the average water temperature of the bottom tanks were also measured using RTDs. Three thermocouples were placed in the bottom water tank, and the average of them was selected as the tank temperature.

The air temperature and humidity of the circulating were measured at the air inlet and outlet. The temperature and humidity were used to measure and record the enthalpy variation of the cooling air across the prototype. The hot water and spray flow rates were monitored using turbine-type flow meters. The hot water flow meter was installed after the hot water pump and before the entrance of the elliptical-tube heat exchanger. The flow meter of the sprinkler loop was installed after the pump and before the water heater. Before and after the placement of a flow meter, a certain length of the pipeline was reserved to ensure stable flow and reduce measurement error. The airflow rate was measured by using a pitot tube and five-point measurements in the air duct. In this study, a high-speed camera was used to capture the water sprinkler and the water film over the tubes. Then, the captured photos were analyzed by an image analysis software. A computer software, IC Measure, was adopted to measure the thickness of the liquid film and the sprinkle characteristics manually. The details of measurement instruments and their specifications are summarized in Table 2.

2.3. Experimental methods and parameters

The experimental parameters of the present study are the airflow rate, sprinkle flow rate, hot water flow rate, and outside air wet-bulb temperature. The experiment was started by inspecting the water tank at the bottom of the prototype to ensure that it is full of water. Then, the electric heater in the heating water tank was turned on, and the hot water circulation was commended by using the pump until the water temperature in the water tank reached 40 °C. At this stage, the exhaust fan and the sprinkler pump were turned on. The next stage was an inspection of the experimental system and thermal insulations.

During the experiment, it was necessary to check the pipeline and the prototype for any water leakage. The removable insulations should also be placed over the prototype to ensure well insulation during the experiment. After confirming that the experimental system was operating normally, the data acquisition device was turned on and checked whether the readings of various measuring instruments are normal. After that, the experimental parameters such as the air, water, and hot water flow rates were set. A notable amount of time was required until the system reaches a steady state. At this stage, the data logger could record the actual measuring data of the experiment. The data logger recorded the data every two seconds for two minutes. Hence, there are 60 records in total, and the average of these data was used for the experimental analyses.

2.4. Experiment procedure

Before starting the experiment, the system must be insulated with

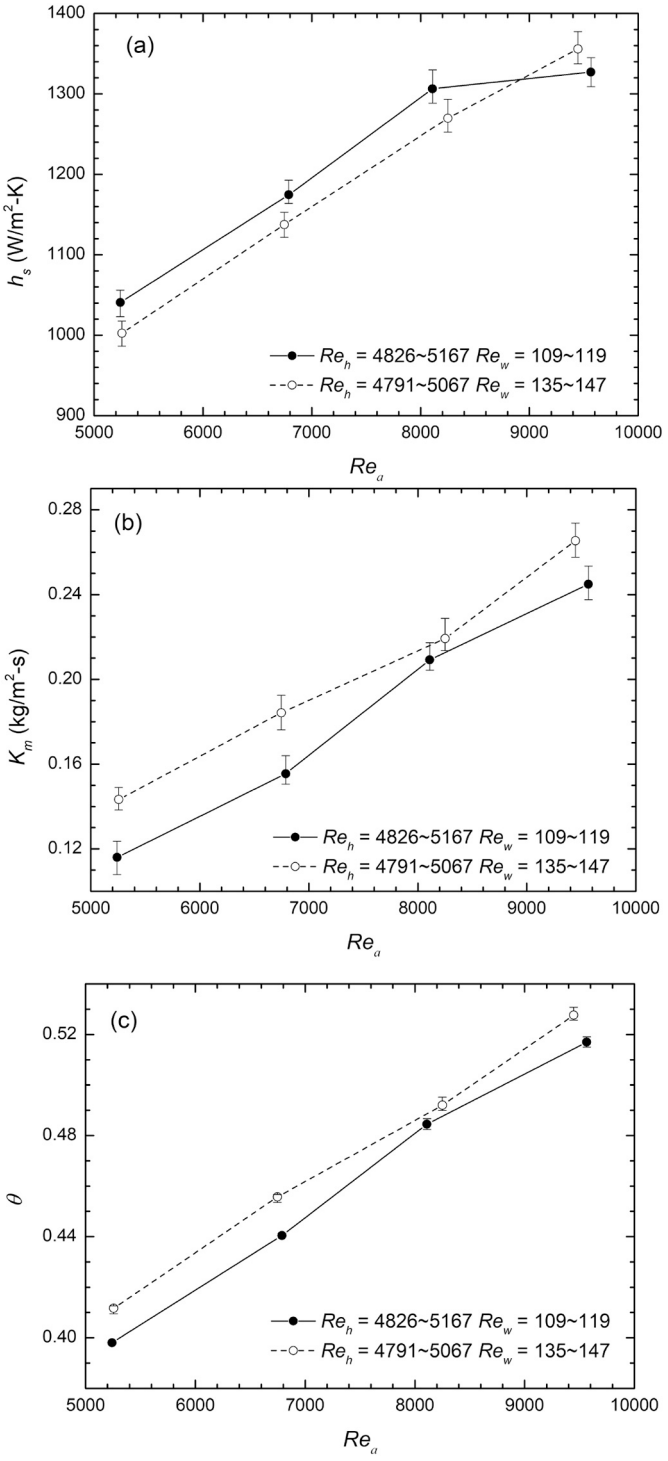

Fig. 4. The influence of air Reynolds number Re_a at different sprinkle water Reynolds number Re_w on the (a) liquid film heat transfer coefficient h_s, (b) mass transfer coefficient K_m, and (c) prototype performance index θ.

insulation materials to avoid heat loss in the experiment; when the experiment is carried out, it is necessary to confirm whether the pipeline and the prototype have water leakage and other conditions that affect the experiment. The experiment begins with turning on the experimental system equipment. The first step is to confirm that the heating tank and the tank at the bottom of the prototype have reached the full water level. Then, the electric heater and hot water pump turn on. The pump circulates the hot water until its temperature rises to 40 °C. At this stage, the exhaust fan and the sprinkle pump turn on cool down the hot water.

After confirming that the experimental system is operating normally, the data capture device and the computer monitor the measured data. The recorded data should be monitored to ensure that the readings of the measuring instruments are normal. If there is an abnormality, confirm whether the circuit is disconnected or whether the measuring instrument is faulty. When the prototype runs normally, the conditions required for the experiment, such as airflow rate, sprinkling water flow rate, hot water flow rate, could be adjusted. Then, the stability of the experimental system should be carefully checked and ensured. Stability is a crucial task, which can impact the accuracy of the experimental analysis. After the experimental conditions are set, the system should continue to operate until the measured values no longer change. After the system is stable, the data extractor starts to record experimental data. It is set to record each data every two seconds. The recording time is two minutes, which leads to a total of 60 records. The average value of the recordings is used as the data required for analysis.

3. Theoretical analysis of experimental data

3.1. The analysis method

The hot water in the elliptical tube conducts the thermal energy to the liquid film outside the tube wall. The liquid film absorbs the thermal energy in the forms of sensible heat and the latent heat of evaporation. Then, the heated liquid film dissipates its heat to the airflow due to the temperature difference between the airflow and the liquid film.

The cooling capacity Q_c of the prototype was calculated as:

$$Q_c = \dot{m}_h \bullet c_{p,w} \bullet \left(T_{h,i} - T_{h,o}\right) \tag{1}$$

where $\dot{m}_h$ is the mass flow rate of hot water in the pipe, $c_{p,w}$ is the average specific heat of hot water, and $T_{h,i}$ and $T_{h,o}$ are the inlet and outlet water temperature of the hot water, respectively. Eventually, the thermal energy of the hot water in the tube was dissipated to the airside. Hence, by using the energy conservation of the system, the total absorbed heat by the airflow (Q_a) is computed as:

$$Q_a = \dot{m}_a \bullet \left(i_{a,2} - i_{a,1}\right) \tag{2}$$

where $\dot{m}_a$ is the mass flow rate of the air, and $i_{a,1}$ and $i_{a,2}$ are the inlet air enthalpy and outlet air enthalpy, respectively.

The temperature of the water film outside the tube is $\overline{T_s}$, which is equal to the average sprinkling temperature, and the heat transfer occurs at a differential area of dA_o on the surface of a tube. Thus, the heat transfer of the liquid film outside the tube dq can be computed as:

$$dq = U_{film} \bullet \left(T_h - \overline{T_s}\right) \bullet dA_o \tag{3}$$

In the above equation, U_{film} is the heat transfer coefficient calculated from the hot water side in the tube to the liquid film outside the tube. Now, in order to compute U_{film}, Eq. (3) was integrated on the overall area of the tubes array (A_o), which yields:

$$U_{film} = \frac{\dot{m}_h \bullet c_{p,w}}{A_o} ln\left(\frac{T_{h,i} - \overline{T_s}}{T_{h,o} - \overline{T_s}}\right) \tag{4}$$

The convective heat transfer coefficient h_h in the tube is calculated by the Gnielinski relations, as follows:

$$f = [1.58ln(Re) - 3.28]^{-2} \tag{5}$$

$$\frac{Nu = (f/2) \bullet (Re - 1000) \bullet Pr}{1.07 + 12.7 \bullet \sqrt{f/2} \bullet (Pr^{2/3} - 1)} \tag{6}$$

$$h_h = \frac{Nu \bullet k}{D} \tag{7}$$

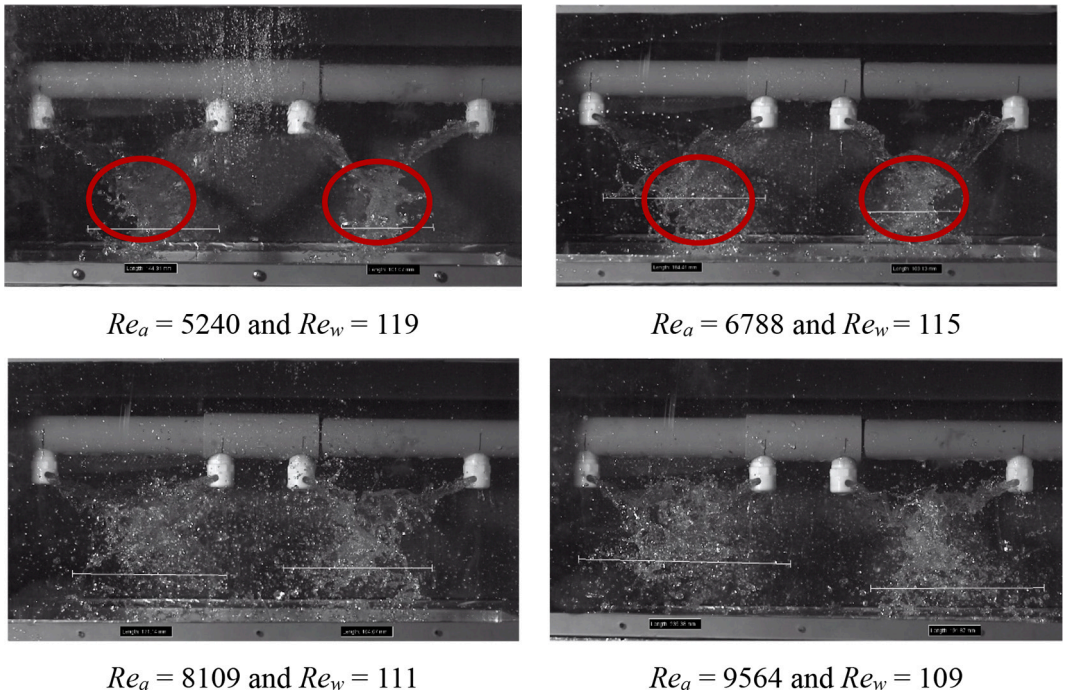

Fig. 5. The sprinkling picture at various upward air Reynolds numbers Re_a and sprinkling water Reynolds numbers Re_w for A nozzle.

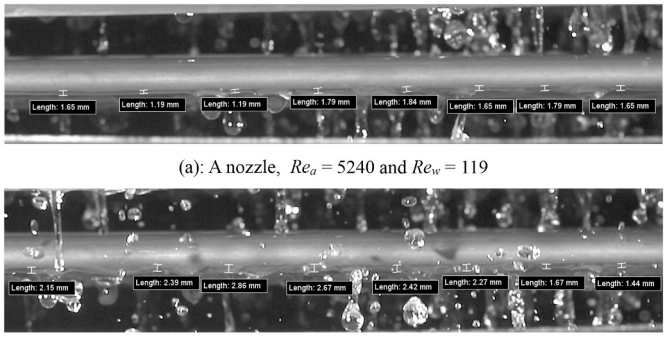

(a): A nozzle, $Re_a = 5240$ and $Re_w = 119$

(b): A nozzle, $Re_a = 5255$ and $Re_w = 147$

Fig. 6. Image of liquid film over tubes for A nozzle.

Table 4
Test conditions and corresponding Re_a, Re_w, Re_h for the study of the A when the nozzle sprinkle flow rate of 50 LPM (60 Hz).

Experiment frequency (Hz)	30	40	50	60
Air volume (CMM)	52.86	67.87	82.88	94.83
Re_a	5255.16	6747.43	8249.98	9445.59
Sprinkle flow rate (LPM)	51.91	52.12	51.68	50.91
Re_w	147.86	144.46	140.14	135.76
Hot water flow rate (LPM)	27.86	27.95	28.00	28.01
Re_h	5067.31	4963.77	4868.48	4791.14
Outside air wet bulb temperature (°C)	23.10	23.12	22.97	22.88

where the above relation is valid in in the following range $0.5 < Pr < 2000$, $3000 < Re < 5{,}000{,}000$.

The convective heat transfer coefficient at the liquid film (h_s) was computed using thermal resistance. The thermal resistance from the hot water side in the tube to the liquid film outside the tube can be expressed as a series of resistances including, the convective thermal resistance of the liquid film, the conductive thermal resistance of the tube wall, and the convective thermal resistance of the hot water in the tube as:

$$\frac{1}{U_{film}} = \frac{1}{h_s} + \frac{d_o ln(d_o/d_i)}{2k_t} + \frac{d_o}{d_i h_h} \tag{8}$$

And consequently, the convective heat transfer coefficient at the liquid film is obtained as:

$$h_s = \left[\frac{1}{U_{film}} - \frac{d_o ln(d_o/d_i)}{2k_t} - \frac{d_o}{d_i h_h}\right]^{-1} \tag{9}$$

The heat transfer process from the water film outside the tube to the air was analyzed by assuming a differential element of the water film outside the tube. The process includes the sensible heat transfer caused by the temperature difference between the liquid-gas interface and the air and the liquid-gas interface. The latent heat transfer, which is the result of the concentration difference from the partial pressure of water vapor in the air, is:

$$dq = \dot{m}_a di_a = h_{sen}\left(T_{a,int} - T_a\right)dA + K_m\left(w_{a,int} - w_a\right)i_{fg,w}dA \tag{10}$$

where $\dot{m}_a$ is the air mass flow rate, $T_{a,\ int}$ is the liquid-gas interface temperature, T_a is the air temperature, $w_{a,\ int}$ the humidity ratio of the liquid-gas interface, and w_a is the humidity ratio of the air. The coefficient of h_{sen} was computed from the definition of the Lewis factor as $h_{sen} = Le_f \times c_{p,\ a} \times K_m$. Thus, Eq. (10) can be re-written as:

$$dq = \frac{h_{sen}}{c_{p,a}}\left[c_{p,a}\left(T_{a,int} - T_a\right) + \left(w_{a,int} - w_a\right)i_{fg,w}\right]dA \tag{11}$$

Now, by using the definition of the mixed air enthalpy, $i_a = i_{a,\ dry} + wi_{g,\ w} = c_{p,\ a}T_a + wi_{g,\ w}$, the dq is obtained as:

$$dq = \dot{m}_a di_a = \frac{h_{sen}}{c_{p,a}}\left(i_{a,int} - i_a\right)dA \tag{12}$$

According to Merkel's assumption for a wet cooling tower, $Le_f = 1$, the air-side heat transfer of the prototype can be expressed as:

$$dq = \dot{m}_a di_a = K_m\left[i_a'\left(\overline{T_s}\right) - i_a\right]dA \tag{13}$$

where $i_a'\left(\overline{T_s}\right)$ is the saturated air enthalpy at the average sprinkler

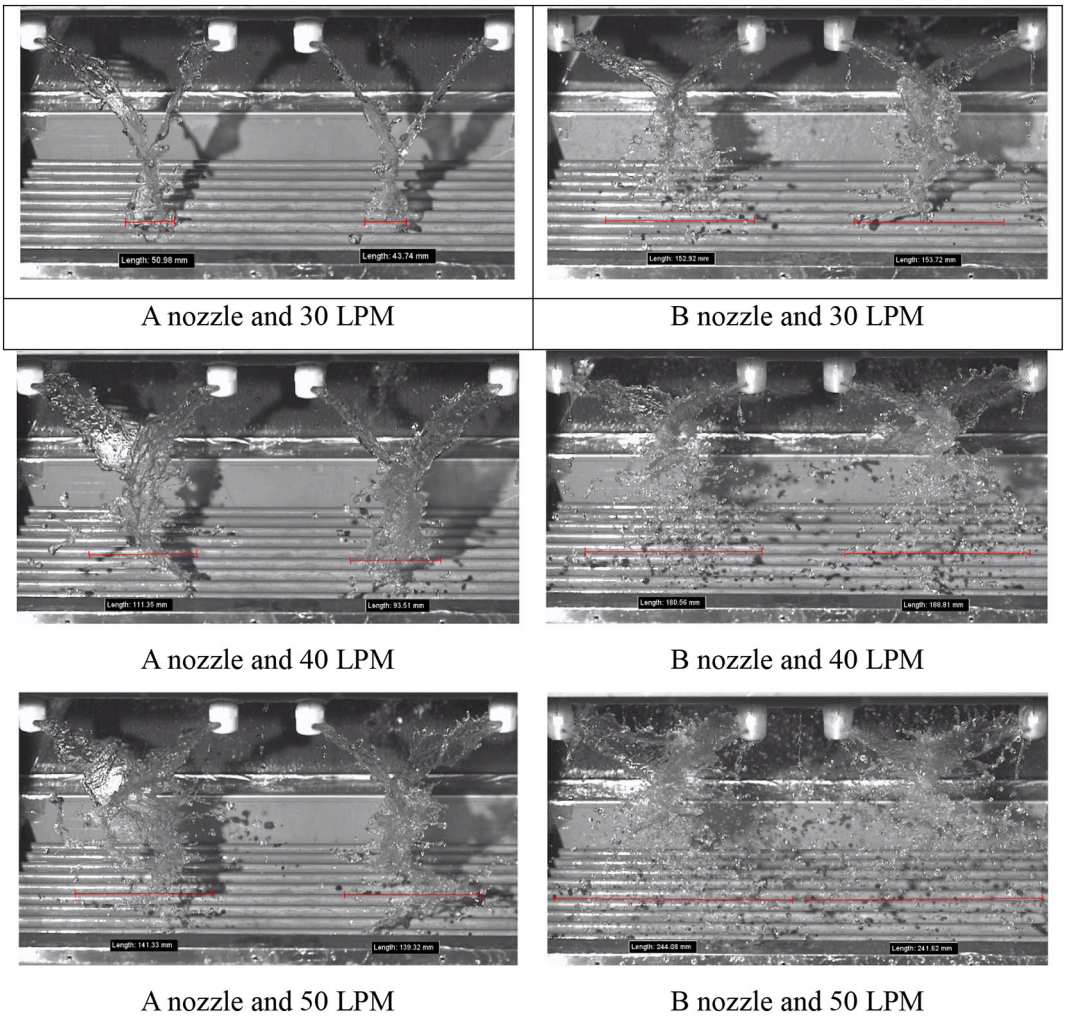

Fig. 7. Image of sprinkling picture over tubes for various sprinkling flow rats and two nozzle types.

Table 5
Test conditions and corresponding Re_a, Re_w, Re_h for the study of the B nozzle when the sprinkling flow rate is about 40 LPM.

Experiment frequency (Hz)	30	40	50	60
Air volume (CMM)	52.74	68.23	81.52	96.20
Re_a	5240.05	6788.04	8109.93	9564.76
Sprinkle flow rate (LPM)	41.51	41.69	41.61	41.50
Re_w	113.08	112.21	109.16	107.39
Hot water flow rate (LPM)	28.02	27.98	27.97	28.00
Re_h	5005.10	4959.27	4832.01	4743.52
Outside air wet bulb temperature (°C)	21.58	22.65	22.40	22.18

Table 6
Test conditions and corresponding Re_a, Re_w, Re_h for the study of the B nozzle when the sprinkling flow rate is about 50 LPM.

Experiment frequency (Hz)	30	35	40
Air volume (CMM)	52.74	68.23	81.52
Re_a	5316.34	6866.17	8228.00
Sprinkle flow rate (LPM)	51.88	52.74	52.46
Re_w	142.04	139.33	135.09
Hot water flow rate (LPM)	27.79	27.86	27.89
Re_h	4979.23	4848.07	4727.93
Outside air wet bulb temperature (°C)	22.70	22.17	21.67

temperature. Integrating Eq. (13) on the overall area of the tubes (A_o),

$$K_m = \frac{\dot{m}_a}{A_o} ln\left[\frac{i_a{}'(\overline{t_s}) - i_{a,1}}{i_a{}'(\overline{t_s}) - i_{a,2}}\right] \tag{14}$$

where $i_{a,\ 1}$ and $i_{a,\ 1}$ are the enthalpy of the air at the inlet and outlet, respectively.

The performance index of the prototype (θ) is introduced as a characteristic parameter to judge the performance index of the prototype as follow:

$$\theta = \frac{T_{h,i} - T_{h,o}}{T_{h,i} - T_{WB,i}} \tag{15}$$

in which $T_{WB,\ i}$ is the wet-bulb temperature of the inlet air. The water evaporation rate of the prototype was obtained from the specific humidity difference between the inlet and outlet of the air and the air mass flow rate $\dot{m}_a$ as:

$$\text{Evaporation rate of sprinkler} = \dot{m}_a\left(w_{a,o} - w_{a,i}\right) \tag{16}$$

where $w_{a,\ o}$ is the specific humidity of the outlet air, and $w_{a,\ i}$ is the specific humidity of the inlet air. Finally, the Reynolds number of the airside, Re_a, is defined as

$$\frac{Re_a = \rho_a \bullet u_{max} \bullet D}{\mu_a} \tag{18}$$

where u_{max} is the airflow velocity in the channel and, ρ_a is the air

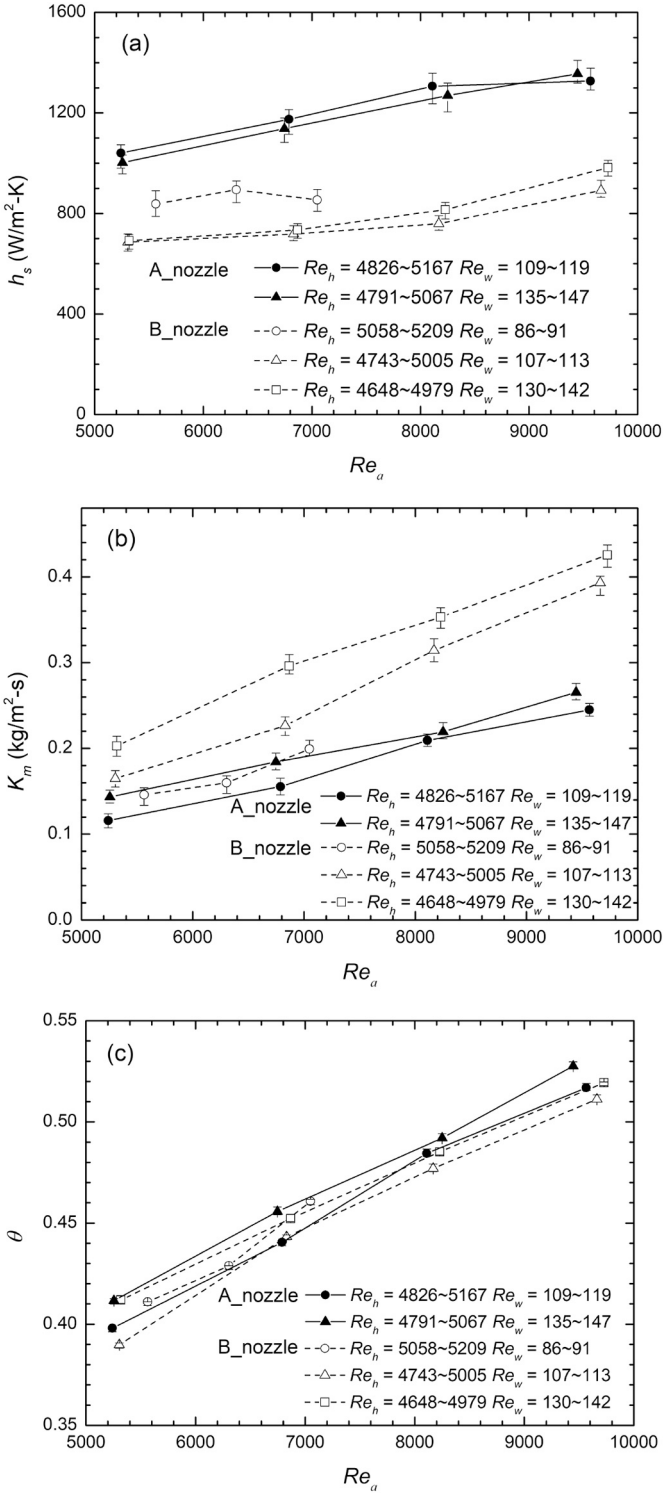

Fig. 8. The influence of nozzle type on the (a) liquid film heat transfer coefficient h_s, (b) mass transfer coefficient K_m, and (c) prototype performance index θ.

density, D is the hydraulic diameter of the elliptical tube, and μ_a is the dynamic viscosity of air. The Reynolds number is introduced as:

$$Re_w = \frac{4\Gamma_w}{\mu_w} \tag{19}$$

where μ_w is the dynamic viscosity of water, and $\Gamma_w = \frac{\dot{m}_w}{2n_r \cdot 2L_t}$. Here, $\dot{m}_w$ is the mass flow rate of the sprinkler (kg/s), and L_t is the length of the tube

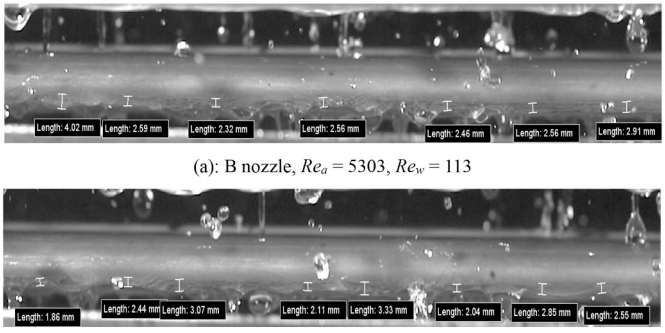

(a): B nozzle, Re_a = 5303, Re_w = 113

(b): B nozzle, Re_a = 5316, and Re_w = 142

Fig. 9. Image of liquid film over tubes for B nozzle.

(m). The coefficient of n_r is the number of tubes in each row of the array. Since the array is staggered, it has been multiplied by 2, i.e., $2n_r$. The Reynolds number at the hot water side was defined as:

$$Re_h = \frac{4\Gamma_h}{\mu_h} \tag{20}$$

where $\Gamma_h = 4\frac{\rho_h Q_h}{\pi D_h}$ in which Q_h is the hot water flow rate in the hot tube, ρ_h is the hot water density, and D_h is the hot water tube's diameter.

3.2. Experimental error analysis

Before commencing the measurements, all of the thermocouples and sensors were calibrated. The error of the thermocouples after calibration was found less than ±0.046 °C. Then the error analysis was calculated using the following formula [33]:

$$\frac{\omega\,(\mathrm{R})}{\mathrm{R}} = \left[\left(\frac{\partial \mathrm{R}}{\partial \mathrm{x}_1}\cdot\frac{\omega(\mathrm{x}_1)}{\mathrm{R}}\right)^2 + \left(\frac{\partial \mathrm{R}}{\partial \mathrm{x}_2}\cdot\frac{\omega(\mathrm{x}_2)}{\mathrm{R}}\right)^2 + \cdots + \left(\frac{\partial \mathrm{R}}{\partial \mathrm{x}_n}\cdot\frac{\omega(\mathrm{x}_n)}{\mathrm{R}}\right)^2\right]^{1/2} \tag{21}$$

where x_1, x_2 … x_n are the independent variables in the experiment; R is the strain number; ω (R) is the error of R.

The heat transfer coefficient (U_{film}) in the experiment is affected by the hot water mass flow rate ($\dot{m}_h$), the hot water inlet temperature ($T_{h,1}$), the hot water outlet temperature ($T_{h,2}$), and the average temperature of the sprinkler ($\overline{T_s}$). The average error of the RTD of the hot water inlet is 0.00121%, the average error of the RTD of the hot water outlet is 0.00387%, and the average error of the sprinkler water RTD is 0.004276%. Substituting various values of errors in Eq. (20) leads to the thermal heat transfer coefficient (U_{film}) with an error of about 3.39%.

The heat exchange errors between the hot water side (Q_c) inside the experimental tube and the air side (Q_a) outside the tube were also computed. The error was within 15%, and the smallest error can reach 1.67%.

3.3. Experimental reproducibility

The experiment's reproducibility was tested under the experimental conditions of B nozzle, sprinkle flow 40 LPM, a range of fan frequencies (30 to 60 Hz), and outside air wet-bulb temperatures. Then, the U_{film} and K_m of the three experiments were compared, respectively. The results confirm that the three experimental curves are all very close, and the maximum error is 6.9% of K_m.

4. Results and discussions

The thermal behavior and performance of the prototype for various test cases are discussed in this section. The impact of air volume rate, sprinkle flow rate, nozzle type, environment air conditions, and the hot

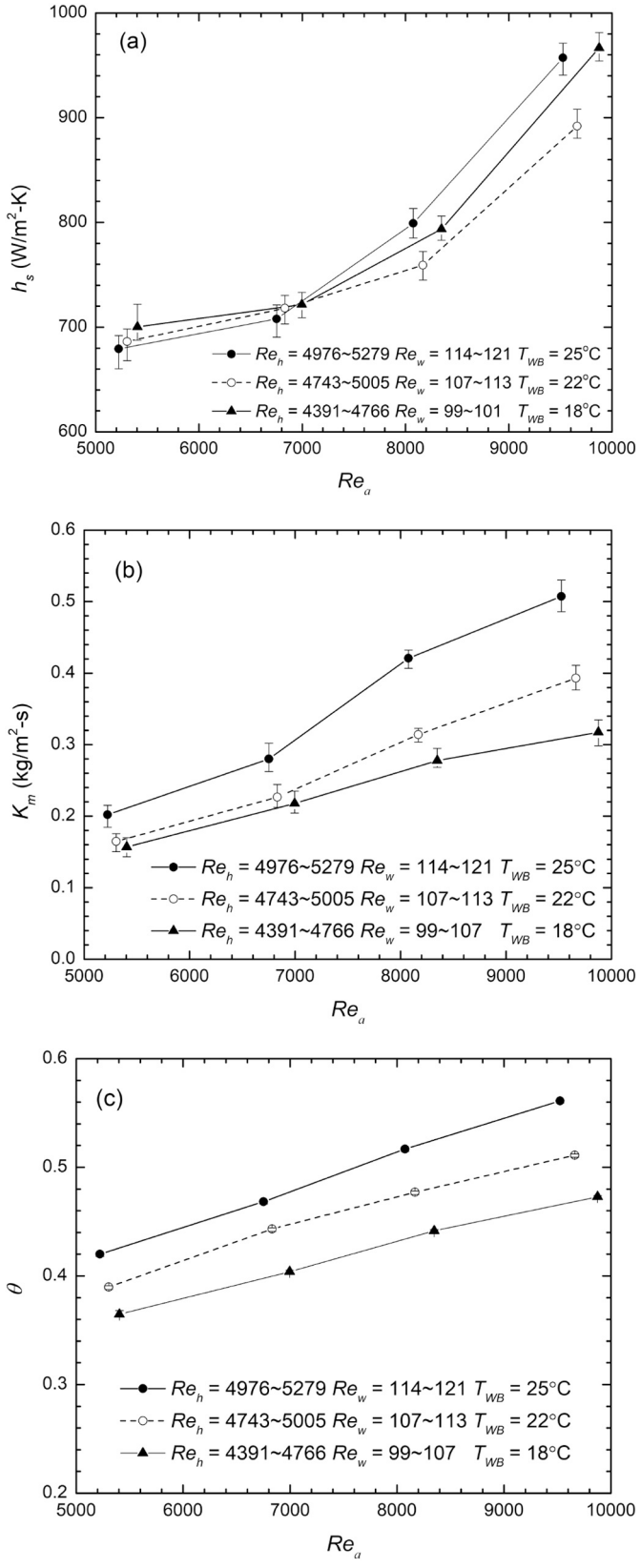

Fig. 10. The influence of outside air wet-bulb temperature on the (a) liquid film heat transfer coefficient h_s, (b) mass transfer coefficient K_m, and (c) prototype performance index θ.

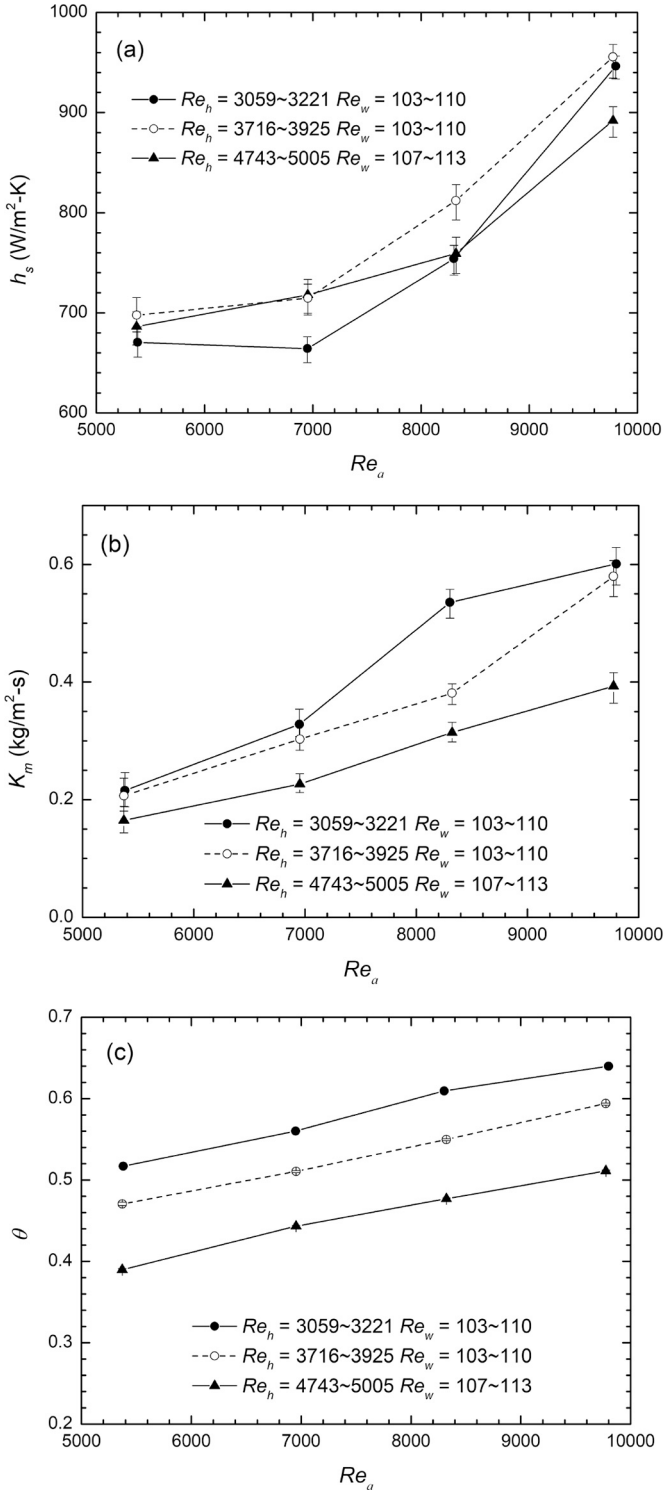

Fig. 11. The influence of hot water flow rate on the (a) liquid film heat transfer coefficient h_s, (b) mass transfer coefficient K_m, and (c) prototype performance index.

water flow rate in the prototype performance are investigated. The heat exchange capacity (Q_c), the variation of hot water temperature, heat transfer coefficient (U_{film}), external film heat transfer coefficient (h_s), mass transfer coefficient (K_m), and performance index of the prototype (θ) are studied.

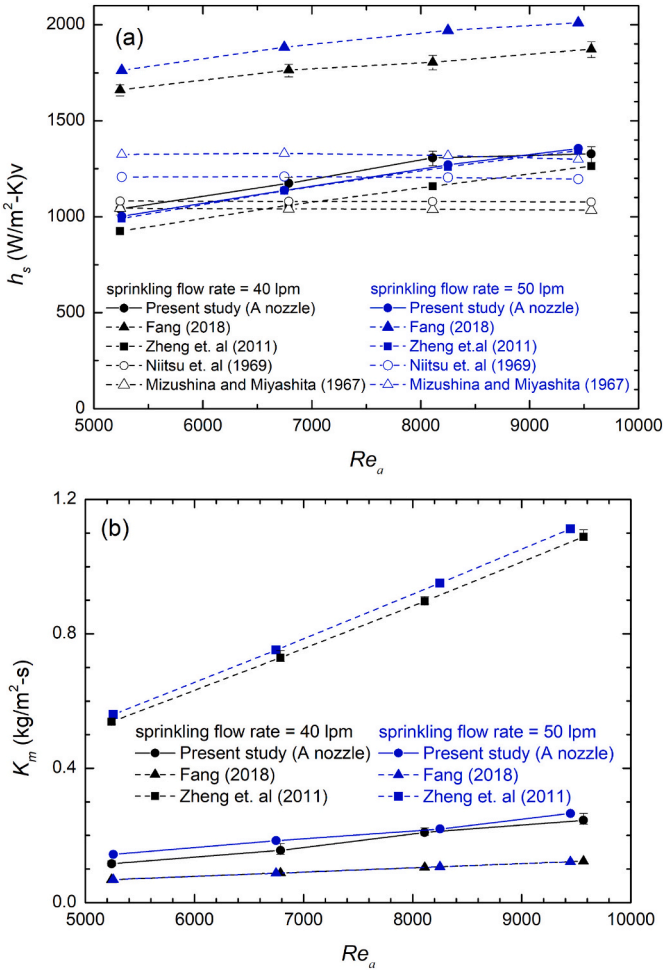

Fig. 12. Comparison of the experimental value of the (a) h_s and (b) K_m with the literature results for A nozzle at two sprinkling flow rates of 40 LPM and 50 LPM.

4.1. Airflow rate and sprinkler flow rate

Here, the hot water flow rate and the sprinkle flow rate were kept constant at 28 LPM and 40 LPM, respectively. The nozzle A was used for sprinkler, and the outside air wet-bulb temperature was 23 °C. The experimental conditions and the Re_a corresponding to different sprinkle water Reynolds number Re_w and hot water Reynolds number Re_h are summarized in Table 3.

The influence of the air Reynolds number Re_a at different sprinkle water Reynolds number Re_w on the liquid film heat transfer coefficient h_s, the mass transfer coefficient K_m and the performance index θ is presented in Fig. 4. It is clear in Fig. 4(a) that the liquid film heat transfer coefficient boosts with increasing air Reynolds number Re_a. In Fig. 4 (b), the mass transfer coefficient K_m is mainly affected by the air Reynolds number Re_a, and the uniformity of the sprinkler on the tube array. When the air Reynolds number Re_a, increases, the impact point of the sprinkler moves upward, which improves the uniformity of the sprinkler on the tube array. Hence, the airflow could forcefully blow through the water droplets. This phenomenon has a significant effect on mass transfer, making the mass transfer coefficient increase sharply with the increase of the air Reynolds number Re_a. Looking at K_m alone is not enough to judge the performance of the prototype; the prototype performance index θ defined by Eq. (15) was used as the performance evaluation standard of the prototype. Fig. 4(c) shows that the increase in air Reynolds number Re_a gradually improves the performance index.

The image of water sprinklings for A nozzle is depicted in Fig. 5 for various upward air Reynolds numbers Re_a. While Fig. 6 illustrates a close view of the liquid film over the tubes for two different sprinkle water Reynolds numbers. The impact point of sprinklers is denoted by a circle in the images for convenience. When airflow rate is low, i.e., $Re_a = 5240$, the impact point of the sprinklers is toward the bottom, resulting in poor uniformity of dispersion after the impact. Hence, it results in a smaller heat transfer coefficient. An increase of the air Reynolds number to $Re_a = 6788$ shifts the impact point of sprinklers upward, which improves the sprinkler uniformity. When the air volume reaches high values of $Re_a = 8109$ and $Re_a = 9564$, a further increase in air Reynolds number does not affect the uniformity of the sprinklers. Here, the hot water flow of rate was fixed at 28 LPM, and the wet-bulb temperature was fixed at 23 °C, while nozzle A was used for water sprinkling. The experiment specifications are summarized in Tables 3 and 4. The results of Tables 3 and 4 were provided with the same conditions but with different sprinkle flow rates of 40 LPM (50 Hz) and 50 LPM (60 Hz), respectively.

The effects of sprinkle water Reynolds number Re_w on the heat transfer coefficient of the liquid film h_s, the mass transfer coefficient K_m and the performance index of the prototype θ are also presented in Figs. 4(a), 4(b) and 4(c), respectively. It is clear that the increase of the sprinkling water Reynolds number reduces the liquid film heat transfer coefficient. This observation is in agreement with the observations of Figs. 6 for liquid layer thickness. Besides, the increase of the sprinkling eater Reynolds number improves the mass transfer coefficient. This is because the K_m is mainly affected by the interaction of airflow and the liquid film. A higher sprinkle water flow rate, better mixing, and uniform liquid film increase the air-liquid interaction, and consequently, the water evaporation. In Figs. 4(c), the performance index in the case of a higher sprinkler flow rate of $Re_w = 147–135$ is better than that of $Re_w = 119–109$, regardless of the amount of air Reynolds number. Although a higher sprinkling flow rate increases the thickness of the liquid film and slightly drops U_{film}, the increase of the mass transfer coefficient is notable. The overall performance index increases by the growth of the sprinkle flow rate.

4.2. Nozzle type

The effect of nozzle types of A and B on the heat and mass transfer was investigated for various sprinkling flow rates and airflow rates when the hot water flow rate was fixed at 28 LPM (hot water pump 30 Hz), and the outside air wet-bulb temperature of 21–23 °C. The sprinkling flow rate was investigated in the range of 30, 40, 50 LPM (sprinkler pump 40, 50, 60 Hz). Moreover, the configuration design of the A nozzle was not suitable for the lower sprinkler flow rate of 30 LPM, and hence, only the B nozzle test was performed at the sprinkler flow rate of 30 LPM.

The images of the sprinkle pictures for the two nozzles are depicted in Fig. 7. The size of the spreading area can judge the uniformity of the sprinkler after the collision. Due to the small internal configuration of the B nozzle, the water pressure inside the nozzle is relatively large, and there is a broad watering range. The water spray's uniformity formed by the B nozzle at a water flow rate of 40 and 50 LPM is better than A nozzle. As seen in the case of A nozzle, the sprinkled water cannot cover a notable number of tubes when the sprinkle flow rate is 30 LPM. The test specifications of using B nozzle are summarized in Tables 5 and 6 for the flow rates of 40 and 50 LPM, respectively. The operative condition of the system can be realized by using the results of these two tables for B nozzle and Tables 3 and 4 for A nozzle. A comparison between the Re_w for A nozzle and B nozzle in these tables shows a slight difference between Reynolds numbers for the same flow rates, while for a constant flow rate, the same Reynolds numbers could be expected. This slight difference is because the circulating pump was controlled by the operating frequency (50 Hz and 60 Hz), and using different nozzles could lead to slightly different flow rates since the exact flow rates were measured by turbine-type flow meters. The actual measurements have been reported in these tables. Thus, the Reynolds numbers are not identical.

Fig. 8 shows the influence of the type of nozzles on the heat and mass transfer under various air Reynolds numbers and sprinkling water Reynolds numbers. In Fig. 8 (a), the lower h_s is noted for B nozzle relatively to that of A nozzle. This can be made plausible by noting Fig. 9 that the B nozzle with better uniformity forms a thick liquid film, which results in lower h_s. The effects of nozzle type on mass transfer coefficient and performance index are plotted in Figs. 8 (b) and (c), respectively. It is noted in Fig. 8 (b) that the mass transfer coefficient K_m using the B nozzle is better than that of A nozzle. This is due to a broader picture of sprinkle water caused by B nozzle. By using B nozzle under the same operating conditions, the uniformity of the sprinkler was improved. However, the performance index of both cases is close to each other. It is worth noticing that B nozzle is applicable for low flow rates, which is a practical advantage.

4.3. Impact of outside air wet-bulb temperature

Fig. 10 presents the influence of outside air wet-bulb temperature on the liquid film heat transfer coefficient h_s, the mass transfer coefficient K_m and the prototype performance index θ. The measured results show that the change of outside air wet-bulb temperature has a slight influence on the liquid film heat transfer coefficient at low air Reynolds number. It is clearly can be found in Fig. 10(b) that the increase in outside wet-bulb temperature promotes the mass transfer coefficient. The higher the outside air wet-bulb temperature, the larger the saturated air diffusion coefficient D at the sprinkler temperature around the tube array. Although the U_{film} change at different outside air wet-bulb temperatures is not substantial, a higher outside air wet-bulb temperature increases the diffusion coefficient D of the saturated air and promotes K_m. Hence, as seen in Fig. 10 (c), the rise of the outside air wet-bulb temperature improves the performance index.

4.4. Hot water flow rate

Effects hot water Reynolds number on the liquid film heat transfer coefficient h_s, the mass transfer coefficient K_m and the prototype performance index are presented in Fig. 11. The variation of hot water temperature on liquid film heat transfer was minimal. Fig. 11 (b) interestingly shows that the mass diffusion coefficient K_m is higher when the hot water Reynolds number is low. This is since, for a low volume rate of hot water, the first array of elliptical tubes next to the entrance is hot, and hence, this hot array boosts the evaporation and, consequently, the mass transfer coefficient. Hence, as depicted in Fig. 11 (c), a lower hot water Reynolds number leads to a better prototype performance index.

4.5. Empirical correlations

The following empirical relations for the heat transfer coefficient of film liquid h_s and mass transfer coefficient K_m were obtained using the experimental data. The empirical relations are a function of the air-side Reynolds number (Re_a), the sprinkle water Reynolds number (Re_w), and the average sprinkle water temperature (T_w).

A nozzle:

$$h_s = 0.1232 \times {Re_a}^{0.6497} \times {Re_w}^{0.0338} \times {T_w}^{0.9723} \quad (21a)$$

$$K_m = 5.3622 \times 10^{-7} \times {Re_a}^{1.2097} \times {Re_w}^{0.4134} \times {T_w}^{3.9087\times10^{-5}} \quad (21b)$$

$5240 \le Re_a \le 9565$, $109 \le Re_w \le 148$, $26 \le T_w \le 31(^{\circ}C)$。.

B nozzle:

$$h_s = 0.9658 \times {Re_a}^{0.5742} \times {Re_w}^{1.6256E-10} \times {T_w}^{0.4884} \quad (22a)$$

$$K_m = 3.1874 \times 10^{-12} \times {Re_a}^{1.7936} \times {Re_w}^{0.9534} \times {T_w}^{1.4378} \quad (22b)$$

$5221 \le Re_a \le 9874$, $86 \le Re_w \le 142$, $21 \le T_w \le 31(^{\circ}C)$.

The error between most of the experimental values and the empirical formula is less than 10%.

4.6. Comparison of experiments and related literature

The experimental results of the liquid film heat transfer coefficient h) and the mass transfer coefficient K_m of the current study are compared with the literature. The specifications of the evaporative cooler in the related literature were shown in Table 1. The applicable range of empirical formulas in related literature is consistent with the h_s and K_m empirical formulas of Zheng et al. [27] and the h_s empirical formulas of Niitsu et al. [34] and Mizushima et al. [35]. The comparison shows that the elliptical shape of tubes significantly influences the thermal behavior of evaporative cooling. A Comparison between the empirical formulas of Fang [36] with similar dimensions and shapes of elliptical tube rows and the present study results shows a notable difference. This difference could be due to the very high Reynolds number of the airside.

Figs. 12(a) and 12 (b) show compassion between h_s and K_m obtained from the present study and the literature results for A nozzle. The results are presented for the sprinkling flow rates of 40 and 50 LPM and various values of air Reynolds number. It is clear in Fig. 12 (a) that the experimental values of h_s for the A nozzle are quite close to the predicted empirical formulas. However, there are some differences between the overall results and the outcomes of the Fang [36]. This difference is due to the large gap between the tubes, which leads to an excessive difference in Reynolds number computation and notable error in the predicted values. However, the trend of the experimental results is similar. The same trend of behavior can be noted for the mass transfer coefficient in Fig. 12 (b).

5. Conclusion

The heat transfer behavior and performance index of an evaporative cooling system (prototype) with an elliptic tube heat exchanger were investigated experimentally. The impact of air, sprinkle water, hot water flow rates, the outside wet bulb temperature, and nozzle type on the heat and mass of the prototype were studied. Empirical corrections for the liquid film heat transfer coefficient and mass transfer coefficient were reported, and the results were compared with the literature results. A good agreement was found with the outcomes of the present study and the previous works. The major findings of the current experimental study can be summarized as follows:

1. With a fixed sprinkle flow rate, the rise of the air Reynolds number improves the sprinkling impact and uniformity of water film over tubes. The increase in the air Reynolds number also boosts the air-liquid interaction and mass transfer coefficient. As a result, the higher the air Reynolds number, the better liquid film heat transfer coefficient h_s, mass transfer coefficient K_m and prototype thermal performance.
2. The increase of the sprinkle water flow rate improves the uniformity of water film over the tubes, but it also grows the thickness of water film over tubes, which eventually reduces *the* h_s. This is while the increase of sprinkle water flow rate improves the water and air interaction and boosts the mass transfer coefficient. As a judgment of improvement of heat transfer, the index of performance was computed. It was found that the rise of the sprinkle water flow rate slightly elevates the index performance.
3. The study of nozzle types shows that the nozzle type can induce a notable influence on the interaction of air and sprinkle water and liquid film formation. The B nozzle with a smaller inner diameter and opening produces a more uniform water sprinkler than A nozzle type. Although the B nozzle type provides a uniform water film and better air-water interaction and mass transfer coefficient K_m, it grows the thickness of the water film and consequently elevates the h_s. The outcomes show that using B nozzle could lead to a slightly better index of performance. Although the improvement of the index of performance θ for the B nozzle is minimal, it could be applied to a low sprinkle water flow rate of 30 LPM and provides a good sprinkler

uniformity. Thus, B nozzle has a certain advantage in practical applications.

4. The rise in the wet-bulb temperature of the outside air elevated the hot water temperature and the and sprinkler temperature. The growth of the sprinkle water temperature increased the saturated air diffusion coefficient around the tube array and lead to a better mass transfer coefficient K_m. The rise of the wet-bulb temperature improved the overall performance index θ.
5. The better overall performance index was noted for a lower hot water Reynolds number.

Declaration of Competing Interest

None.

Acknowledgments

The authors appreciate the financial support from Ministry of Science and Technology, Taiwan, under grant number MOST 108-3116-F-027-001. The authors also acknowledge the financial support by the "Research Center of Energy Conservation for New Generation of Residential, Commercial, and Industrial Sectors" from The Featured Areas Research Center Program within the framework of the Higher Education Sprout Project by the Ministry of Education (MOE) in Taiwan.

References

[1] S.H. Bayoumy, S.M. El-Marsafy, T.S. Ahmed, Optimization of a saturated gas plant: meticulous simulation-based optimization–a case study, J. Adv. Res. 22 (2020) 21–33.
[2] B. Saleh, Parametric and working fluid analysis of a combined organic Rankine-vapor compression refrigeration system activated by low-grade thermal energy, J. Adv. Res. 7 (5) (2016) 651–660.
[3] M.G. Salim, Selection of groundwater sites in Egypt, using geographic information systems, for desalination by solar energy in order to reduce greenhouse gases, J. Adv. Res. 3 (1) (2012) 11–19.
[4] T.J. Moses, Indirect evaporative cooling system with supplemental chiller that can be bypassed, in, Google Patents, 2018.
[5] M. Bourgeois, System and Method for Evaporative Cooling of a Heated Apparatus, in, Google Patents, 2019.
[6] J. Wang, Q. Meng, L. Zhang, Y. Zhang, B.-J. He, S. Zheng, M. Santamouris, Impacts of the water absorption capability on the evaporative cooling effect of pervious paving materials, Build. Environ. 151 (2019) 187–197.
[7] Y. Zhang, L. Zhang, Z. Pan, Q. Meng, Y. Feng, Y. Chen, Hydrological properties and solar evaporative cooling performance of porous clay tiles, Constr. Build. Mater. 151 (2017) 9–17.
[8] R. Boukhanouf, A. Alharbi, H.G. Ibrahim, O. Amer, M. Worall, Computer modelling and experimental investigation of building integrated sub-wet bulb temperature evaporative cooling system, Appl. Therm. Eng. 115 (2017) 201–211.
[9] T.A. Ndukaife, A.A. Nnanna, Optimization of water consumption in hybrid evaporative cooling air conditioning systems for data center cooling applications, Heat transfer engineering 40 (7) (2019) 559–573.
[10] C. Yang, Z. Yi, L. Haibo, M. Xiaoping, S. Jun, Application of a New Evaporative Cooling Tower in Underground Engineering, Contamination Control & Air-Conditioning Technology 2, 2017, p. 24.
[11] W.A. Olosunde, A.K. Aremu, D.I. Onwude, Development of a solar powered evaporative cooling storage system for tropical fruits and vegetables, Journal of Food Processing and Preservation 40 (2) (2016) 279–290.
[12] S. Shao, H. Liu, H. Zhang, C. Tian, Experimental investigation on a loop thermosyphon with evaporative condenser for free cooling of data centers, Energy 185 (2019) 829–836.
[13] P.M. Cuce, S. Riffat, A state of the art review of evaporative cooling systems for building applications, Renew. Sust. Energ. Rev. 54 (2016) 1240–1249.
[14] F. Kojok, F. Fardoun, R. Younes, R. Outbib, Hybrid cooling systems: a review and an optimized selection scheme, Renew. Sust. Energ. Rev. 65 (2016) 57–80.
[15] D.K. Sharma, R. Sharma, Application of evaporative condenser in energy saving and performance improvement of domestic air conditioner: a review, International Journal of Production Engineering 2 (2) (2016) 20–27.
[16] Y. Yang, G. Cui, C.Q. Lan, Developments in evaporative cooling and enhanced evaporative cooling-a review, Renew. Sust. Energ. Rev. 113 (2019) 109230.
[17] B. Porumb, P. Ungureşan, L.F. Tutunaru, A. Şerban, M. Bălan, A review of indirect evaporative cooling technology, Energy Procedia 85 (2016) 461–471.
[18] I. Abd Manaf, F. Durrani, M. Eftekhari, A review of desiccant evaporative cooling systems in hot and humid climates, Advances in Building Energy Research (2018) 1–42.
[19] M.W. Shahzad, K. Thu, Y.-d. Kim, K.C. Ng, An experimental investigation on MEDAD hybrid desalination cycle, Appl. Energy 148 (2015) 273–281.
[20] K.C. Ng, K. Thu, S.J. Oh, L. Ang, M.W. Shahzad, A.B. Ismail, Recent developments in thermally-driven seawater desalination: energy efficiency improvement by hybridization of the MED and AD cycles, Desalination 356 (2015) 255–270.
[21] M.W. Shahzad, K.C. Ng, K. Thu, B.B. Saha, W.G. Chun, Multi effect desalination and adsorption desalination (MEDAD): a hybrid desalination method, Appl. Therm. Eng. 72 (2) (2014) 289–297.
[22] M.W. Shahzad, M. Burhan, L. Ang, K.C. Ng, Energy-water-environment nexus underpinning future desalination sustainability, Desalination 413 (2017) 52–64.
[23] A. Hasan, K. Siren, Theoretical and computational analysis of closed wet cooling towers and its applications in cooling of buildings, Energy and buildings 34 (5) (2002) 477–486.
[24] J. Facao, A.C. Oliveira, Thermal behaviour of closed wet cooling towers for use with chilled ceilings, Appl. Therm. Eng. 20 (13) (2000) 1225–1236.
[25] J. Heyns, D. Kröger, Experimental investigation into the thermal-flow performance characteristics of an evaporative cooler, Appl. Therm. Eng. 30 (5) (2010) 492–498.
[26] A. Hasan, K. Siren, Performance investigation of plain circular and oval tube evaporatively cooled heat exchangers, Appl. Therm. Eng. 24 (5–6) (2004) 777–790.
[27] W.-Y. Zheng, D.-S. Zhu, J. Song, L.-D. Zeng, H.-j. Zhou, Experimental and computational analysis of thermal performance of the oval tube closed wet cooling tower, Appl. Therm. Eng. 35 (2012) 233–239.
[28] M. Sarker, E. Kim, C. Moon, J. Yoon, Performance characteristics of the hybrid closed circuit cooling tower, Energy and Buildings 40 (8) (2008) 1529–1535.
[29] R. Niu, S. You, Q. Chen, F. Ma, Modeling and performance analysis of the closed cooling tower, Journal of Shenyang Jianzhu University (Natural Science) 3 (2007).
[30] Q. Zhu, B. Zhang, Q. Chen, C. He, D.C. Foo, J. Ren, H. Yu, Model reductions for multiscale stochastic optimization of cooling water system equipped with closed wet cooling towers, Chem. Eng. Sci. 224 (2020) 115773.
[31] M.H. Nugraha, Experimental and simulation study on the performance of counter flow closed cooling tower systems, International Journal of Technology 6 (3) (2015) 365–379.
[32] M. Rashidinejad, R. Maddahian, A. Abbasian Arani, Experimental and numerical study of closed circuit wet cooling tower and heat transfer coefficients calculation on the outer surface of hot water tubes, Modares Mechanical Engineering 20 (4) (2020) 901–913.
[33] J. Holman, W. Gajda, Experimental methods for engineers Ch. 3, McGraw-Hill, New York, 1994.
[34] Y. Niitsu, K. Naito, T. Anzai, Studies on characteristics and design procedure of evaporative coolers, Journal of SHASE 43 (7) (1969) 581–590.
[35] T. Mizushima, R. Ito, H. Miyashita, Experimental study of an evaporative cooler, Int. Chem. Eng. 7 (4) (1967) 727.
[36] J.C. Fang, An Experimental Study of Evaporative Coolers Using Elliptic Tubes, National Taipei University of Technology, Taipei, Taiwan, 2018.
[37] A. Hasan, K. Siren, Performance investigation of plain and finned tube evaporatively cooled heat exchangers, Appl. Therm. Eng. 23 (3) (2003) 325–340.